Coordination Among Neural Modules Through a Shared Global Workspace

Anirudh Goyal [1] **Aniket Didolkar** [1] **Alex Lamb** [1] **Kartikeya Badola** [1] **Nan Rosemary Ke** [1 2] **Nasim Rahaman** [1 3]
Jonathan Binas [1] **Charles Blundell** [2] **Michael Mozer** [4] **Yoshua Bengio** [1]

Abstract

Deep learning has seen a movement away from representing examples with a monolithic hidden state towards a richly structured state. For example, Transformers segment by position, and object-centric architectures decompose images into entities. In all these architectures, interactions between different elements are modeled via pairwise interactions: Transformers make use of self-attention to incorporate information from other positions; object-centric architectures make use of graph neural networks to model interactions among entities. However, pairwise interactions may not achieve global coordination or a coherent, integrated representation that can be used for downstream tasks. In cognitive science, a *global workspace* architecture has been proposed in which functionally specialized components share information through a common, bandwidth-limited communication channel. We explore the use of such a communication channel in the context of deep learning for modeling the structure of complex environments. The proposed method includes a shared workspace through which communication among different specialist modules takes place but due to limits on the communication bandwidth, specialist modules must compete for access. We show that capacity limitations have a rational basis in that (1) they encourage specialization and compositionality and (2) they facilitate the synchronization of otherwise independent specialists.

1. Introduction

Deep Learning has seen a movement towards more structured models with cleaner separation between different pieces of information often handled by different components. The induced structure, and separation of knowledge has improved generalization, model-size scaling, and long-range dependencies (Berner et al., 2019; Vinyals et al., 2019; Brown et al., 2020). This opens up questions about how to achieve coherence and coordination between different components in such architectures. Looking back to the 1980s, the focus in AI was much less on learning and more on constructing articulated, multi-component architectures and examining how intelligence might emerge from interactions among this collection of simple, functionally specialized components (Fodor, 1983; Braitenberg, 1986; Minsky, 1988; Brooks, 1991). Each of these specialist modules is on the scale of a typical component of a computer program, like a subroutine that implements a narrow, prespecified function from certain input contents to certain output contents.[1] Through appropriate communication and coordination, a set of specialists can achieve complex, dynamic, and flexible behavior patterns.

As a concrete illustration, consider the task of driving a car in terms of specialists. One specialist might monitor the position of the car with respect to lines on the road, and another specialist might adjust the steering direction based on the perceptual data. In addition, there might be specialists which provide alerts when certain events occur, such as loud sounds, reaching a critical intersection on a route, or coming into close proximity to the car in front. To execute the task of driving the car properly, all these specialists need to interact coherently and broadcast their individual information to each other.

Arguably, modern ML and AI has yet to develop broad architectural frameworks for learning both the specialist modules and how they should *interact*, while the classical view lacks an articulate story about how learning could take place successfully in such frameworks. In this article, we revisit this classical view with modern machine learning tools based on end-to-end learning and differentiable memory and attention mechanisms. Inspired by the Global Workspace Theory (Baars, 1993; Dehaene et al., 1998; Shanahan & Baars, 2005; Shanahan, 2006; 2010; 2012; Dehaene et al., 2017) from cognitive neuroscience, we argue that flexibility

[1]Mila, University of Montreal [2]Deepmind [3]Max Planck Institute, Germany [4]Google Brain. Correspondence to: Anirudh Goyal <anirudhgoyal9119@gmail.com>.

[1]In the literature, specialists are sometimes referred to as processes or agents.

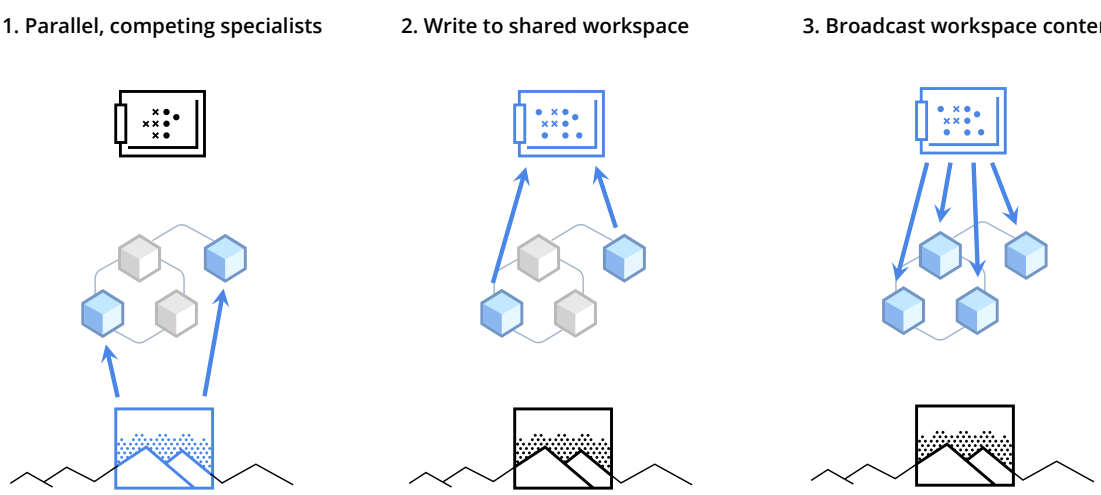

Figure 1. **Step 1:** an ensemble of specialist modules doing their own default processing; at a particular computational stage, depending upon the input, a subset of the specialists becomes active. **Step 2:** the active specialists get to write information in a shared global workspace. **Step 3:** the contents of the workspace are broadcast to all specialists.

and generalization emerge through an architecture of specialists if their training encourages them to communicate effectively with one another via the bottleneck of a shared workspace (figure 1).

Distributed specialist modules. From a computational perspective, articulated multi-component architectures composed of sparsely interacting specialist modules show desirable scaling properties (e.g., more specialists can seamlessly be added), increased robustness (the system can tolerate the removal of individual specialists), and efficiency (information is processed predominantly locally, reducing the cost of communication between specialists). However, modularization also requires mechanisms to establish sharing of compatible representations across specialists. While portions of a task might be solved by independent specialists, synchronization is critical particularly when there are statistical, functional, or causal dependencies among the specialists.

Coherence through a shared workspace. In cognitive neuroscience, the Global Workspace Theory (GWT) (Baars, 1993; Dehaene et al., 2017) suggests an architecture allowing specialist modules to interact. The key claim of GWT is the existence of a shared representation—sometimes called a blackboard, sometimes a workspace—that can be modified by any specialist and that is broadcast to all specialists, along with the notion that write access is limited to maintain coherence. Our interpretation of this restriction on write access is that it stems from an assumption on the form of the joint distribution between high-level concepts. In this paper, we explore a communication and coordination scheme similar to the one proposed by GWT for modern neural network architectures like Transformers (Vaswani et al., 2017; Dehghani et al., 2018; Parmar et al., 2018; Radford et al., 2019; Brown et al., 2020) and attention-based modular architectures (Goyal et al., 2019; Rahaman et al., 2020; Mittal et al., 2020; Goyal et al., 2020; Madan et al., 2021).

In terms of our driving example, the workspace could be used to override default behaviors by giving high priority to specialist modules which provide alerts of various sorts (loud sounds, presence of a child on the street), allowing specialists which respond to such alerts to take control of behavior over default driving routines. This scenario implies that prioritization of signals in a shared workspace is critical.

A shared communication channel necessitates common representations. For a multitude of specialist modules to cooperate, a common language is necessary (Baars, 1997). For example, in the driving scenario, alerts may come from auditory or visual processing specialists, but regardless of the source, a signal for danger must be placed in the workspace to override default behavior, whether that behavior is controlled by a radio-tuning specialist or a steering specialist. Although specialist modules can be pre-wired to have compatible communication interfaces, we will model an architecture in which an ensemble of specialist modules is *trained in coordination*, which should lead to a shared language (Colagrosso & Mozer, 2005). Internally, individual specialists can use whatever form of representations that serves them, but their inputs and outputs require alignment with other specialists in order to synchronize. For example, an unusual event such as a rough thud under the wheels might not have been previously experienced, but the mere signalling of novelty could override default specialists. Without a global communication channel, specialists would have to learn to communicate through pairwise interactions, which might limit coordination of behavior in novel situ-

ations: global communication ensures exchangeability of knowledge to achieve systematic generalization.

2. Synchronizing neural modules through a shared workspace

We investigate a neural architecture reminiscent of the GW model, where a number of sparsely communicating specialist modules interact via a shared working memory. In particular, we extend the Transformer (Vaswani et al., 2017), attention and slot-based modular architectures (Goyal et al., 2019) by adding a shared workspace and allowing modules (each representing an entity) to compete for write access in each computational stage.

$$\text{Attention}(Q, K, V) = \text{softmax}\left(\frac{QK^T}{\sqrt{d}}\right)V,$$

Key-value attention. Key-value attention defines the backbone of updates to the hidden states in the proposed model. This form of attention is widely used in self-attention models and performs well on a wide array of tasks (Bahdanau et al., 2014; Vaswani et al., 2017; Santoro et al., 2018). Key-value attention selects an input value based on the match of a query vector to a key vector associated with each value. To allow differentiability and thus easier learnability, selection is soft and computes a convex combination of all the values. Such a mechanism makes it possible to change on-the-fly both the source of input and how the shared workspace is updated. It changes the way to think of the outputs of specialists and the elements of the memory: they should be considered as an *unordered* set of elements to be selected by an attention mechanism from the contents of specialists. More precisely, soft attention uses the product of a *query* (represented as a matrix Q of dimensionality $N_r \times d$, with N_r queries, and d the dimension of each query) with a set of N_o objects each associated with a *key* as a row in matrix K^T ($N_o \times d$). After normalization with a softmax the resulting convex weights are used to combine the *values* V_i (row i of matrix V): where the softmax is applied to each row of its argument matrix, yielding a set of convex weights. For our experiments, we use multihead dot product attention.

Neural modules with pairwise interactions. Our approach to synchronizing neural modules is highly general and mostly agnostic to the task, domain, or specific choice of architecture, with the only requirement being that the model consists of multiple specialist modules which either operate independently or have sparse interactions requiring to only match pairs of modules at a time. Our goal is to explore how introducing a shared workspace can help these modules to become better synchronized and coordinated. We show the utility of the shared workspace for synchronization in (a) Transformers (Vaswani et al., 2017), in which all interactions between positions are performed via attention, and (b) slot-based architectures like Recurrent Independent Mechanisms or RIMs (Goyal et al., 2019) in which all pairwise interactions between modules are performed via attention. In the context of slot-based architectures, each slot's content is associated with a specialist module, whereas in Transformers different entities each associated with a different position acts as a specialist module (figure 2).

Both Transformers and RIMs utilize a self-attention mechanism for sharing information between modules, typically implemented in a pairwise manner, i.e., each specialist attends to every other specialist. Instead, we facilitate information sharing among specialist modules through a *limited capacity shared workspace*. In this framework at each computational stage, different specialists compete for write access to the common workspace. The contents of the workspace, in turn, are broadcast to all specialist modules simultaneously.

Notation. The input is processed through a sequence of computational stages indexed by t, and at each stage, n_s entities are operated on (i.e., n_s different modules in slot-based architectures like RIMs or n_s different positions in the case of Transformers). Each of these n_s specialist modules has a distinct internal n_h-dimensional state $\boldsymbol{h}_t^k$, for $k \in \{1, ..., n_s\}$. The specialist modules communicate with each other via a shared workspace divided into n_m memory *slots*, each consisting of a vector of n_l elements, denoted $\boldsymbol{M} = [\boldsymbol{m}_1; \ldots \boldsymbol{m}_j; \ldots \boldsymbol{m}_{n_m}]$. The shared workspace is updated across different computational stages i.e., different timesteps in recurrent architecture and different layers in the case of Transformers. At each computational stage t, different specialists compete for writing in the shared workspace, but all specialists can read from the current state of the workspace. In the case of an autoregressive task, we can restrict the information sharing to previous positions and keep a separate version of the workspace for each position.

2.1. Specifics of the Shared Workspace.

Step 1: Process Input to obtain an entity representation for each specialist. The first step is external to the proposed method, and involves processing the input to form the initial representation vector for each of the different specialists. Different common deep learning architectures can be used to form the representation of different specialists. For example, Transformers start with a matrix $n_s \times n_h$ whose rows are initialized as the n_h-dimensional embeddings of the input at each position of the sequence. Slot-Based Recurrent architectures like RIMs consist of a single-layer recurrent structure where the hidden state $\mathbf{h}_t$ at computational stage t is decomposed into the substates of the n_s specialists, $\mathbf{h}_t^k$ for $k = 1, ...n_s$.

In the proposed scheme within each computational stage, the updates of the hidden state of different specialists follow

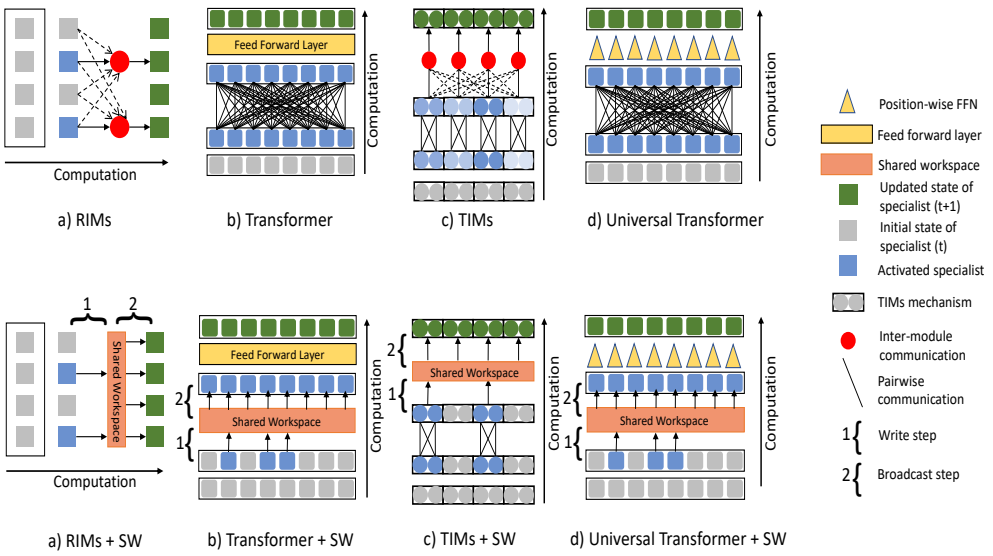

Figure 2. **Using a Shared Workspace for creating global coherence in RIMs, Transformers, TIMs and Universal Transformers (UT).** (Top Half) All four of these architectures use pairwise communication (using key-value attention) to establish coherence between individual specialist modules. In the case of RIMs (Goyal et al., 2019) and TIMs (Lamb et al., 2021), these specialists are independent modules which compete with each other in order to take control over the state update based on a given input. In the case of Transformers (Vaswani et al., 2017) and Universal Transformers (Dehghani et al., 2018), each specialist is associated with a different position. Activated specialists are denoted by a blue shade and the intensity depends on the degree of activation. In the case of Universal Transformers, the state update dynamics for each position is shared across all layers and all positions (denoted by a yellow triangle). (Bottom Half) We replace pairwise communication with a shared workspace to create *global coherence* between different specialists. Communication using the shared workspace is a two-step process (as denoted by 1 and 2 in the figures). In the first step (1), specialists compete for write access to the shared workspace, resulting in a subset of them being activated (in blue), and only the activated specialists perform the write operation on the workspace. In the second step (2), the contents of the shared workspace are broadcast to all the specialists.

a two-step process. First, specialists compete and write to a shared workspace. Second, information from the workspace gets broadcast to all the specialists, as explained next.

Step 2: Writing Information in the shared workspace. The specialists compete to write into the shared workspace, whose contents need to be updated in the context of new information received from different specialists. This step ensures that only the critically important signals make it to the shared workspace and therefore prevents the workspace from being cluttered. Let matrix $\boldsymbol{R}$ represent the combined state of all the specialists (i.e. $h_t^k \quad \forall k \in \{1, \ldots, n_s\}$ as the rows of $\boldsymbol{R}$). In order to implement the competition between specialists to write into the workspace, we use a key-query-value attention mechanism. In this case, the query is a function of the state of the memory matrix $\boldsymbol{M}$ (with one row per slot of the memory), i.e $\widetilde{\boldsymbol{Q}} = \boldsymbol{M}\widetilde{\boldsymbol{W}}^q$. Keys and values are a function of the information from the specialists i.e., a function of $\boldsymbol{R}$. We apply dot product attention to get the updated memory matrix: $\boldsymbol{M} \leftarrow \text{softmax}\left(\frac{\widetilde{\boldsymbol{Q}}(\boldsymbol{R}\widetilde{\boldsymbol{W}}^e)^{\mathrm{T}}}{\sqrt{d_e}}\right)\boldsymbol{R}\widetilde{\boldsymbol{W}}^v$. The use of a regular softmax to write into $\boldsymbol{M}$ leads to a standard soft competition among different specialists to write in the shared workspace. One can also use a top-k softmax (Ke et al., 2018) to select a fixed number of specialists allowed to write in the shared workspace: based on the pre-softmax values, a fixed number of k specialists which have the highest values are selected, and get access to write in the shared workspace. Selection with a top-k softmax is a hybrid between hard and soft selection. We denote the set of thus selected specialists as $\mathcal{F}_t$. We note that we can apply the attention mechanism multiple times to distill information from different specialists into the shared workspace. Here, the contents of the shared workspace are updated in the gated way as proposed in RMC (Santoro et al., 2018). We ask the reader to refer to appendix section C for more details.

Step 3: Broadcast of information from the shared workspace. Each specialist then updates its state using the information broadcast from the shared workspace. We again utilize an attention mechanism to perform this consolidation. All the specialists create queries $\widehat{\boldsymbol{q}}_k = \boldsymbol{h}_t^k\widehat{\boldsymbol{W}}^q$, which are matched with the keys $\widehat{\boldsymbol{\kappa}}_j = (\boldsymbol{m}_j\widehat{\boldsymbol{W}}^e)^{\mathrm{T}} \quad \forall k \in \{1, \ldots, n_s\},\ j \in \{1, \ldots, n_m\}$ from the updated memory slots, forming attention weights $s_{k,j} = \text{softmax}\left(\frac{\widehat{\boldsymbol{q}}_k\widehat{\boldsymbol{\kappa}}_j}{\sqrt{d_e}}\right)$.

The memory slot values generated by each slot of the shared workspace and the attention weights are then used to update the state of all the specialists: $\boldsymbol{h}_t^k \leftarrow \boldsymbol{h}_t^k + \sum_j s_{k,j} \widehat{\boldsymbol{v}}_j$ where $\widehat{\boldsymbol{v}}_j = \boldsymbol{m}_j \widehat{\boldsymbol{W}}^v \quad \forall k \in \{1, \ldots, n_s\}$. After receiving the broadcast information from the workspace, each specialist update their state by applying the dynamics function i.e., one step update of LSTM or GRU units in the case of recurrent architectures, and feedforward layer in the case of Transformers. This yields the new value $\boldsymbol{h}_{t+1}^k$ for the k-th specialist, from which we start the next stage $(t+1)$.

Persistence of shared workspace throughout an episode. The shared workspace is written into and its contents are updated after every stage, i.e., every time-step in a recurrent network and after every layer in Transformers. The contents of the shared memory are only reset at the end of an episode (i.e., at the end of the sequence for RNNs and after the final layer for Transformers).

Computational Complexity of using shared workspace for synchronizing different specialists. To encourage a coherent global coordination, Transformers and slot-based recurrent architectures rely on pairwise interactions captured via an attention mechanism. Unfortunately, such attention mechanisms scale quadratically with the number of specialists. Here, we propose a method which uses a shared workspace to create global coherence between different specialists and in the process, replaces the pair-wise interactions of conventional dot-product attention. The computational complexity of the proposed method is *linear* in the number of specialists. In our experimentation, the number of memory slots is practically constant, which suggests a very favourable scaling behavior, and certainly much less than quadratic. As a point of reference, what would correspond to the number of slots in human working memory (Baars, 1993) is indeed very small (less than 10).

3. Related Work

This work taps into a line of reasoning put forward by historical works, such as (Minsky, 1988; Braitenberg, 1986; Fodor, 1983), wherein it is argued that in order to be able to deal with a wide spectrum of conditions and tasks, an intelligent system should be comprised of many interacting specialized modules or programs, rather than a single "one-size-fits-all" entity. While modular architectures have been the subject of a number of research directions, (Jacobs et al., 1991; Bottou & Gallinari, 1991; Ronco et al., 1997; Reed & De Freitas, 2015; Andreas et al., 2016; Rosenbaum et al., 2017; Fernando et al., 2017; Shazeer et al., 2017; Rosenbaum et al., 2019; Goyal & Bengio, 2020), we focus here on a mechanism for achieving coherence and synchronization between specialist modules via a global workspace shared between all specialists.

Prior works have explored incorporating slot-based memory in the context of recurrent neural networks (Graves et al., 2014; 2016; Santoro et al., 2018). In the context of transformers, Burtsev & Sapunov (2020) introduce *memory tokens* that are processed in addition to sequence tokens, whereas Dai et al. (2019) (Transformer-XL) propose to partition a long sequence to smaller segments and use the activations of the previous segment in memory while processing the current segment. Building on the latter, Rae et al. (2019) propose to store activations from prior segments in a compressed memory. However, these methods do not restrict memory writes to be sparse and competitive. Further, deploying a shared workspace to establish coherence between different specialists as opposed to using all-pair communication has an added benefit, in that it allows us to tackle the $O(n^2)$ complexity of self-attention. This makes our work related to previous work on reducing the computational complexity of dot product attention in Transformers. Lee et al. (2019) introduce the *ISAB* module, which maps between sets and comprises two dot-product attention layers. In the first layer, a set of trainable parameters are used as queries and the elements of the input set as keys; in the second layer, the output of the first layer is used as keys and the input set as queries. However, unlike in this work, the intermediate states (corresponding to the output of the first layer) are not maintained across layers. Longformer (Beltagy et al., 2020) proposes to restrict attention to a local receptive field, hence making complexity linear (although at the cost of missing long-range dependencies). The Routing Transformer (Roy et al., 2020) uses K-means clustering to group together keys and queries and restricts attention locally, leading to an overall complexity of $O(n^{1.5})$. Wang et al. (2020); Katharopoulos et al. (2020) proposed a method to reduce the complexity of self-attention to linear (with some additional differences) in sequence length, and shows that the method achieves results on par with standard Transformer models. We show that using the cognitively inspired shared workspace, we can achieve better results than standard Transformer models, while reducing the complexity of self-attention to be linear in sequence length.

4. Experiments

Here we briefly outline the tasks on which we applied the idea of the shared workspace and direct the reader to the appendix for full details on each task and details on hyperparameter settings for the model. The experiments have the following goals: (a) Demonstrate that the use of the shared workspace can improve results on a wide array of challenging benchmark tasks, with the goal of demonstrating the practical utility and breadth of the technique. (b) Show that the shared workspace addresses coherence between different specialists by achieving improved performance without requiring all pairwise interactions.

4.1. Making sense of the visual input.

Using a shared workspace introduces a bottleneck in sharing of information between specialists. Since the size of the workspace is limited and generally much lower than the number of specialists, there is a limit to the amount of information that can be exchanged among specialists. We hypothesize that mediating communication through a limited capacity workspace should encourage the model to look at relevant information that is important for the downstream objective. We test this hypothesis on a set of visually challenging benchmarks. For our experiments, we use either Transformers or RIMs as a backbone. We first experimented with a 4-layered Transformer with shared parameters across layers as a backbone architecture, as in universal transformers (Dehghani et al., 2018). We replace the pairwise interactions (self-attention) in the baseline Transformer with a shared workspace as described in the previous section. We consider variants of Transformers based on different subsets of important properties. *Transformers* [TR]: Self-attention based multi-layer architecture (Vaswani et al., 2017) with shared parameters across layers. *Sparse Transformers* [STR]: Transformers with sparse factorizations of the attention matrix (Child et al., 2019). *High Capacity Transformers* [TR+HC]: Same as TR but with different parameters across layers. *Transformers with Shared Workspace with soft-competition* [TR+SSW]: Transformers with different positions competing with each other to write in shared workspace using soft-competition. *Transformers with Shared Workspace with top-k competition* [TR+HSW]: Transformers with different positions competing with each other to write in shared workspace using top-k competition. For a more detailed description of all the tasks described below, we ask the reader to appendix section D.

Detecting Equilateral Triangles. To test our hypothesis in an easy to visualize and understand setting, we use a simple toy task where the model is tasked with detecting equilateral triangles in images (Ahmad & Omohundro, 2009). Each image is of size 64×64 and contains 3 randomly placed clusters of points. For equilateral triangles, the midpoints of these clusters are equidistant from each other. This is a binary classification task where the model has to predict whether the three given clusters form an equilateral triangle or not. To feed an image into a Transformer, we follow the same methodology as used in vision Transformers (Dosovitskiy et al., 2020). We first divide an image into equal sized 4×4 patches and treat each patch as a different input position of the Transformer.

To solve this task correctly, the model only needs to attend to relevant information i.e., to patches that contain the cluster of points. Therefore, using a limited capacity shared workspace should be useful here. Our results (presented in figure 3) confirm our hypothesis. We can see that *Transformers with shared workspace attention converge much faster and reach higher accuracy as compared to the baseline Transformer*.

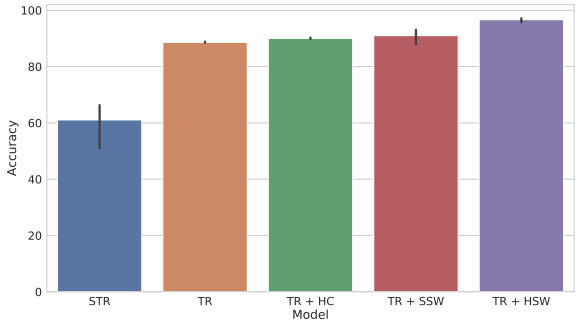

Figure 3. **Detecting Equilateral Triangles.** Here, we compare the performance of the Transformers with shared workspace to other Transformer baselines. Here, we plot the test accuracy for each model.

CATER: Object Tracking. Cater is a spatio-temporal reasoning video dataset introduced in Girdhar & Ramanan (2019). Each video contains 3D objects organized in a 6×6 grid. Each object affords certain actions that can be performed on them. These actions result in movement of the concerned objects and change in their positions. Some of these actions include: *rotate*, *pick-place*, *slide*, *contain*. Throughout the duration of the video, a number of these actions are performed to get the final state of the grid. Note that only a single object undergoes an action, at any instant. The task that we focus on here is called *localization*. In this task, the goal is to predict the location of the target object in the final frame. In this case the target object is called a snitch. The snitch as well as the other objects move across the 6×6 grid. In some scenarios, the snitch may be covered by other objects hence hiding it from the view. In such cases, tracking the movement of the snitch across frames becomes essential. Therefore, capturing long-range temporal dependencies is essential to solve this task.

We first sample frames from the video at a sampling rate S, in this case we use $S = 6$. We pass each sampled frame through a resnet block to get a sequence of feature representations: $\{\boldsymbol{f}_1, \boldsymbol{f}_2, \boldsymbol{f}_3, \ldots, \boldsymbol{f}_T\}$. We then pass this sequence through a Transformer. This task is setup as a classification task where we have to predict which cell in the 6×6 grid contains the snitch in the final frame.

The information exchange limit enforced by the limited capacity of the shared workspace should be useful here as well. For CATER, in some frames the snitch is not visible as it is covered by other objects. Therefore, ideally the model only needs to attend to frames in which the snitch is visible. Additionally, if the snitch is visible throughout the video in all frames, then to accurately predict the final position of the snitch, the model only needs to attend to the final frame

Model	Top-1 %	Top-5 %
STR	$70.6_{\pm 0.08}$	$87.33_{\pm 0.06}$
TR	$70.83_{\pm 0.44}$	$87.8_{\pm 0.08}$
TR + HC	$70.17_{\pm 0.31}$	$88.33_{\pm 0.2}$
TR + HSW (OURS)	$71.07_{\pm 0.04}$	$88.6_{\pm 0.49}$
TR + SSW (OURS)	$71.33_{\pm 0.34}$	$88.3_{\pm 0.05}$

Table 1. **Comparison on CATER Object Tracking**. Here, we compare the Top-1 and Top-5 accuracy of Transformers with shared workspace and Transformers with self-attention. We can see that Transformers with a shared workspace outperform those with pairwise self-attention.

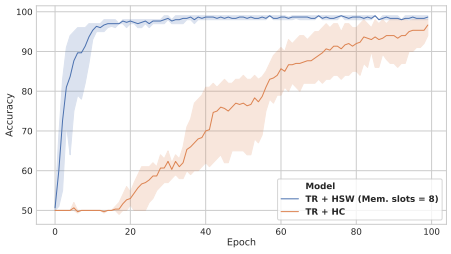

(a) **Non-Relational Questions**

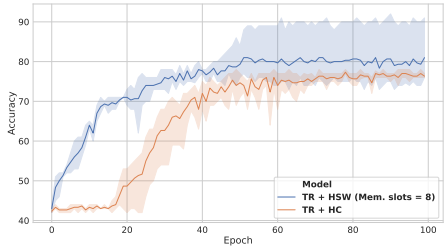

(b) **Relational Questions**

Figure 4. **Comparison on Sort-of-CLEVR relational reasoning**. Speed of convergence for relational and non-relational questions in the sort-of-clevr dataset. We can see that the proposed model converges much faster than the baseline in both cases.

of the video and can completely ignore the initial frames.

The results for this task are presented in table 1. We also experimented with both soft competition TR+SSW and hard competition TR+HSW, with only $k = 5$ specialists writing into the shared workspace. We can see that models with a shared workspace outperform those with pairwise multihead attention thus confirming our hypothesis about the benefits of a shared workspace for this task.

Relational Reasoning : Sort-of-CLEVR. In relational reasoning, the model is tasked with answering questions about certain properties of various objects and their relations with other objects. The model is presented with an image and a question for that image. This task has a clear sparse structure as in order to answer the questions correctly, it needs to only reason about a specific subset of objects that the question mentions. For this task, we use the Sort-of-CLEVR dataset (Santoro et al., 2017).

Each image in Sort-of-CLEVR is a size 75×75 image containing 6 randomly placed geometrical shapes of 6 possible colors and 2 possible shapes. Each image comes with 10 relational questions and 10 non-relational questions. Non-relational questions only consider properties of individual objects. For example, *what is the shape of the red object?* is a non-relational question. On the other hand, relational questions consider relations among multiple objects. For example, *what is the shape of the object closest to the red object?* is a relational question.

The input to the model consists of the image and the corresponding question. We first obtain a sequence of equal-sized patches for the image as in vision Transformers (Dosovitskiy et al., 2020). We concatenate the resulting patch sequence with the representation of the question and pass the combined sequence through the Transformer. Sort-of-CLEVR has a finite number of possible answers, hence this task is setup as a classification task.

We present the results for this task in figure 4. We observe that *the Transformers with the shared workspace converge faster and outperform the baselines for relational as well as non-relational questions*. The superior performance of shared memory can be attributed to the inherent sparsity of this task. For instance, in non-relational questions, the model only needs to attend to a single object referenced in the question to answer it correctly and relational questions only consider a few subset of objects in the image, thus sparsity is helpful for both these types of questions. Therefore, the limited capacity of the shared workspace forces the model to attend to only relevant information.

4.2. Shared Workspace for Physical Reasoning task.

In this task, the trajectory of a number of objects interacting through elastic collisions has to be predicted. In order to solve this task, a coherent picture of where which objects will collide needs to be established by the learner. We use the bouncing-ball dataset from Van Steenkiste et al. (2018). The dataset consists of 50,000 training examples and 10,000 test examples showing $\sim$50 frames of either 4 solid balls bouncing in a confined square geometry, 6-8 balls bouncing in a confined geometry, or 3 balls bouncing in a confined geometry with a random occluded region. In all cases, the balls bounce off the wall as well as off one another. We train baselines as well as the proposed shared workspace extension (e.g., RIMs + SW). As shown in Fig. 5, we study the performance of the proposed model compared with LSTM, RIMs and RMC. The first 10 frames of ground truth are fed in and then the system is rolled out for the next 35 time steps. During the rollout phase, *the proposed method performs better than the baselines in accurately*

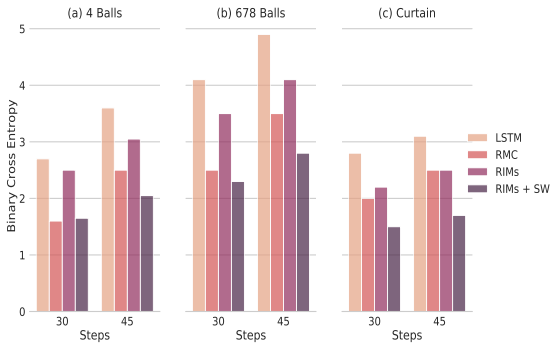

Figure 5. **Bouncing ball motion:** Prediction error comparison of the proposed method, LSTM, RIMs and RMC baseline. Given 10 frames of ground truth, the model predicts the rollout over the next 35 steps. Here, we present the BCE for the 30th frame and 45th frame. The *proposed SW extension performs better than other baselines in accurately predicting the dynamics, with an increasing advantage as the number of unrolled steps (30 vs 45) and balls ((a) vs (b)) increases.* Results are an average over 5 random seeds.

predicting the dynamics of the balls as reflected by cross entropy (CE). For more details, we ask the reader to refer to appendix section F.

4.3. Shared Workspace for Multiagent Starcraft World Modelling.

The SC2 domain (Samvelyan et al., 2019) is a multi-agent reinforcement learning benchmark, wherein teams of heterogeneously typed units must defeat a team of opponents in combat. Each unit type has its own characteristics, e.g. maximum *health*, *shields*, weapon abilities (*cool-down*, *damage per second*, *splash damage*, etc), and strengths (vulnerabilities) against (towards) other unit types, making the world-modeling more challenging.

Task Description. Given observations $\boldsymbol{O}_t^a$ from a team of cooperating agents indexed by a and with positions $\boldsymbol{x}_t^a$ and actions $\boldsymbol{u}_t^a$, predict the observation $\boldsymbol{O}_{t'}^q$ that would be made by an agent q at time $t' = t + 1$ if it were previously at position $\boldsymbol{x}_t^q$. In this environment, **(a)** all agents a have a well-defined and known location $\boldsymbol{x}_t^a$ (at time t), **(b)** the agents' actions $\boldsymbol{u}_t^a$ are local, in that their effects propagate away (from the agent) only at a finite speed, **(c)** the observations are local and centered around agents, in the sense that the agent only observes the events in its local vicinity, i.e., $\boldsymbol{O}_t^a$.

Dataset (Rahaman et al., 2020). The observations $\boldsymbol{O}_t^a$ and actions $\boldsymbol{u}_t^a$ are both multi-channel images represented in polar coordinates centered around the agent position $\boldsymbol{x}_a^t$. The field of view (FOV) of each agent is therefore a circle of fixed radius centered around it. The channels of this multi-channel images correspond to **(a)** a binary indicator marking whether a position in FOV is occupied by a living friendly agent (*friendly marker*), **(b)** a categorical indicator marking the type of living units at a given position in FOV (*unit-type marker*), and **(c)** four channels marking the health, energy, weapon-cooldown and shields (*HECS markers*) of all agents in FOV. With a heuristic, we gather a total of 9K trajectories $(\{\boldsymbol{x}_t^a, \boldsymbol{O}_t^a, \boldsymbol{u}_t^a\}_{a=1}^A)_{t=1}^{100}$ spread over three training *scenarios*, corresponding to `1c3s5z`[2], `3s5z` and `2s5z` in Samvelyan et al. (2019). In addition, we also sample 1000 trajectories (each) from two OOD scenarios `1s2z` and `5s3z`.

Table 2. **Multiagent Starcraft World Modelling:** Performance metrics on `1s2z` and `5s3z` The metrics are: unit-type macro F1 score (UT-F1), friendly-marker F1 score (FM-F1), HECS Negative Mean Squared Error (NMSE) and Log Likelihood (LL). (larger numbers are better) . Results are average over 3 random seeds.

	UT-F1	FM-F1	NMSE	LL
`1s2z task`				
RIMs	$0.5693_{\pm 0.02}$	$0.8135_{\pm 0.03}$	-0.0053	$-0.0532_{\pm 0.004}$
LSTM	$0.6267_{\pm 0.03}$	$0.8464_{\pm 0.02}$	-0.0040	$-0.0382_{\pm 0.006}$
RIMs + SW	$0.6867_{\pm 0.02}$	$0.8532_{\pm 0.01}$	-0.0034	$-0.0321_{\pm 0.004}$
`5s3z task`				
RIMs	$0.453_{\pm 0.01}$	$0.6935_{\pm 0.01}$	-0.028	$-0.154_{\pm 0.01}$
LSTM	$0.497_{\pm 0.03}$	$0.7123_{\pm 0.02}$	-0.013	$-0.125_{\pm 0.02}$
RIMs + SW	$0.538_{\pm 0.01}$	$0.7402_{\pm 0.02}$	-0.013	$-0.119_{\pm 0.01}$

Evaluation Criteria. We report the F1 scores for binary friendly markers, multi-class (macro) F1 score for unit-type markers, negative mean squared error for HECS markers.

Results: Table. 2 shows the performance of the RIMs with workspace as compared with the regular RIMs with self-attention (Goyal et al., 2019) (1200 hidden units, and 12 modules), as well as with LSTM network (1200 hidden units). As shown in Tab. 2, RIMs with pairwise interactions between different specialists perform poorly on this task. *RIMs where a shared workspace is used as a communication channel are able to achieve much better results as compared with LSTMs as well as regular RIMs, thus showing the validity of the proposed idea to establish coherence between different specialists*. For more details regarding the architecture and details about baselines and the proposed method, we ask the reader to refer to appendix, section G.

5. Conclusion

Inspired by cognitive neuroscience global workspace theories, we have proposed a shared workspace model for establishing coherence among modular neural specialists while exchanging information. We show that using a limited capacity shared workspace as a bottleneck for mediating communication among specialists results in better performance across a wide range of visual reasoning benchmarks as compared with the pairwise interactions typically used in self-attention schemes. All communication occurs through key-value attention, which ensures that the specialists are interchangeable, and that any specialist can pass informa-

[2]Here, the code `1c3s5z` refers to a scenario where each team comprises 1 *colossus* (`1c`), 3 *stalkers* (`3s`), and 5 *zealots* (`5z`).

tion to the workspace in form that others can learn to interpret. Experiments on prediction and visual reasoning tasks highlight the advantages brought by the conjunction of modularity and the shared workspace. The proposed model combines several key properties: knowledge and expertise is divided among specialists, they compete to post new contents to the workspace, and after being updated, the shared workspace is accessible to all specialists for their own updates.

6. Acknowledgements

The authors would like to thank Murray Shanahan, Phanideep Gampa, Chen Sun, Bernhard Scholkopf for useful discussions. The authors would also like to thank David Reitter, Dianbo Liu, Guillaume Dumas for useful feedback on the earlier version of the paper.

References

Ahmad, S. and Omohundro, S. Equilateral triangles: A challenge for connectionist vision. 2009.

Andreas, J., Rohrbach, M., Darrell, T., and Klein, D. Neural module networks. In *Proceedings of the IEEE Conference on Computer Vision and Pattern Recognition*, pp. 39–48, 2016.

Baars, B. J. *A cognitive theory of consciousness*. Cambridge University Press, 1993.

Baars, B. J. In the theatre of consciousness. global workspace theory, a rigorous scientific theory of consciousness. *Journal of Consciousness Studies*, 4(4):292–309, 1997.

Bahdanau, D., Cho, K., and Bengio, Y. Neural machine translation by jointly learning to align and translate. *arXiv preprint arXiv:1409.0473*, 2014.

Beltagy, I., Peters, M. E., and Cohan, A. Longformer: The long-document transformer. *arXiv preprint arXiv:2004.05150*, 2020.

Berner, C., Brockman, G., Chan, B., Cheung, V., Dębiak, P., Dennison, C., Farhi, D., Fischer, Q., Hashme, S., Hesse, C., et al. Dota 2 with large scale deep reinforcement learning. *arXiv preprint arXiv:1912.06680*, 2019.

Bottou, L. and Gallinari, P. A framework for the cooperation of learning algorithms. In *Advances in neural information processing systems*, pp. 781–788, 1991.

Braitenberg, V. *Vehicles: Experiments in synthetic psychology*. MIT press, 1986.

Brooks, R. A. Intelligence without representation. *Artificial intelligence*, 47(1-3):139–159, 1991.

Brown, T. B., Mann, B., Ryder, N., Subbiah, M., Kaplan, J., Dhariwal, P., Neelakantan, A., Shyam, P., Sastry, G., Askell, A., et al. Language models are few-shot learners. *arXiv preprint arXiv:2005.14165*, 2020.

Burtsev, M. S. and Sapunov, G. V. Memory transformer. *arXiv preprint arXiv:2006.11527*, 2020.

Child, R., Gray, S., Radford, A., and Sutskever, I. Generating long sequences with sparse transformers. *arXiv preprint arXiv:1904.10509*, 2019.

Colagrosso, M. D. and Mozer, M. C. Theories of access consciousness. In Saul, L. K., Weiss, Y., and Bottou, L. (eds.), *Advances in Neural Information Processing Systems 17*, pp. 289–296. MIT Press, 2005. URL http://papers.nips.cc/paper/2715-theories-of-access-consciousness.pdf.

Dai, Z., Yang, Z., Yang, Y., Carbonell, J., Le, Q. V., and Salakhutdinov, R. Transformer-xl: Attentive language models beyond a fixed-length context. *arXiv preprint arXiv:1901.02860*, 2019.

Dehaene, S., Kerszberg, M., and Changeux, J.-P. A neuronal model of a global workspace in effortful cognitive tasks. *Proceedings of the national Academy of Sciences*, 95(24): 14529–14534, 1998.

Dehaene, S., Lau, H., and Kouider, S. What is consciousness, and could machines have it? *Science*, 358(6362): 486–492, 2017.

Dehghani, M., Gouws, S., Vinyals, O., Uszkoreit, J., and Kaiser, Ł. Universal transformers. *arXiv preprint arXiv:1807.03819*, 2018.

Dosovitskiy, A., Beyer, L., Kolesnikov, A., Weissenborn, D., Zhai, X., Unterthiner, T., Dehghani, M., Minderer, M., Heigold, G., Gelly, S., et al. An image is worth 16x16 words: Transformers for image recognition at scale. *arXiv preprint arXiv:2010.11929*, 2020.

Fernando, C., Banarse, D., Blundell, C., Zwols, Y., Ha, D., Rusu, A. A., Pritzel, A., and Wierstra, D. Pathnet: Evolution channels gradient descent in super neural networks. *arXiv preprint arXiv:1701.08734*, 2017.

Fodor, J. A. *The modularity of mind*. MIT press, 1983.

Girdhar, R. and Ramanan, D. CATER: A diagnostic dataset for compositional actions and temporal reasoning. *CoRR*, abs/1910.04744, 2019. URL http://arxiv.org/abs/1910.04744.

Goyal, A. and Bengio, Y. Inductive biases for deep learning of higher-level cognition. *arXiv preprint arXiv:2011.15091*, 2020.

Goyal, A., Lamb, A., Hoffmann, J., Sodhani, S., Levine, S., Bengio, Y., and Schölkopf, B. Recurrent independent mechanisms. *arXiv preprint arXiv:1909.10893*, 2019.

Goyal, A., Lamb, A., Gampa, P., Beaudoin, P., Levine, S., Blundell, C., Bengio, Y., and Mozer, M. Object files and schemata: Factorizing declarative and procedural knowledge in dynamical systems. *arXiv preprint arXiv:2006.16225*, 2020.

Graves, A., Wayne, G., and Danihelka, I. Neural turing machines. *CoRR*, abs/1410.5401, 2014. URL http://arxiv.org/abs/1410.5401.

Graves, A., Wayne, G., Reynolds, M., Harley, T., Danihelka, I., Grabska-Barwińska, A., Colmenarejo, S. G., Grefenstette, E., Ramalho, T., Agapiou, J., et al. Hybrid computing using a neural network with dynamic external memory. *Nature*, 538(7626):471–476, 2016.

Hochreiter, S. and Schmidhuber, J. Long short-term memory. *Neural computation*, 9(8):1735–1780, 1997.

Jacobs, R. A., Jordan, M. I., Nowlan, S. J., and Hinton, G. E. Adaptive mixtures of local experts. *Neural computation*, 3(1):79–87, 1991.

Karpathy, A. karpathy/mingpt, Aug 2020. URL https://github.com/karpathy/minGPT.

Katharopoulos, A., Vyas, A., Pappas, N., and Fleuret, F. Transformers are rnns: Fast autoregressive transformers with linear attention. In *International Conference on Machine Learning*, pp. 5156–5165. PMLR, 2020.

Ke, N. R., GOYAL, A. G. A. P., Bilaniuk, O., Binas, J., Mozer, M. C., Pal, C., and Bengio, Y. Sparse attentive backtracking: Temporal credit assignment through reminding. In *Advances in neural information processing systems*, pp. 7640–7651, 2018.

Kingma, D. and Ba, J. Adam: A method for stochastic optimization. *arXiv preprint arXiv:1412.6980*, 2014a.

Kingma, D. P. and Ba, J. Adam: A method for stochastic optimization. *arXiv preprint arXiv:1412.6980*, 2014b.

Lamb, A., He, D., Goyal, A., Ke, G., Liao, C.-F., Ravanelli, M., and Bengio, Y. Transformers with competitive ensembles of independent mechanisms, 2021. URL https://openreview.net/forum?id=1TIrbngpW0x.

Lee, J., Lee, Y., Kim, J., Kosiorek, A., Choi, S., and Teh, Y. W. Set transformer: A framework for attention-based permutation-invariant neural networks. In *International Conference on Machine Learning*, pp. 3744–3753, 2019.

Madan, K., Ke, N. R., Goyal, A., Schölkopf, B., and Bengio, Y. Meta attention networks: Meta-learning attention to modulate information between recurrent independent mechanisms. In *International Conference on Learning Representations*, 2021. URL https://openreview.net/forum?id=Lc28QAB4ypz.

Minsky, M. *Society of mind*. Simon and Schuster, 1988.

Mittal, S., Lamb, A., Goyal, A., Voleti, V., Shanahan, M., Lajoie, G., Mozer, M., and Bengio, Y. Learning to combine top-down and bottom-up signals in recurrent neural networks with attention over modules. In *International Conference on Machine Learning*, pp. 6972–6986. PMLR, 2020.

Ott, M., Edunov, S., Baevski, A., Fan, A., Gross, S., Ng, N., Grangier, D., and Auli, M. fairseq: A fast, extensible toolkit for sequence modeling. In *Proceedings of NAACL-HLT 2019: Demonstrations*, 2019.

Parmar, N., Vaswani, A., Uszkoreit, J., Kaiser, L., Shazeer, N., Ku, A., and Tran, D. Image transformer. In *International Conference on Machine Learning*, pp. 4055–4064. PMLR, 2018.

Paszke, A., Gross, S., Massa, F., Lerer, A., Bradbury, J., Chanan, G., Killeen, T., Lin, Z., Gimelshein, N., Antiga, L., Desmaison, A., Kopf, A., Yang, E., DeVito, Z., Raison, M., Tejani, A., Chilamkurthy, S., Steiner, B., Fang, L., Bai, J., and Chintala, S. Pytorch: An imperative style, high-performance deep learning library. In Wallach, H., Larochelle, H., Beygelzimer, A., d'Alché-Buc, F., Fox, E., and Garnett, R. (eds.), *Advances in Neural Information Processing Systems 32*, pp. 8024–8035. Curran Associates, Inc., 2019.

Radford, A., Wu, J., Child, R., Luan, D., Amodei, D., and Sutskever, I. Language models are unsupervised multitask learners. *OpenAI blog*, 1(8):9, 2019.

Rae, J. W., Potapenko, A., Jayakumar, S. M., and Lillicrap, T. P. Compressive transformers for long-range sequence modelling. *arXiv preprint arXiv:1911.05507*, 2019.

Rahaman, N., Goyal, A., Gondal, M. W., Wuthrich, M., Bauer, S., Sharma, Y., Bengio, Y., and Schölkopf, B. S2rms: Spatially structured recurrent modules. *arXiv preprint arXiv:2007.06533*, 2020.

Reed, S. and De Freitas, N. Neural programmer-interpreters. *arXiv preprint arXiv:1511.06279*, 2015.

Ronco, E., Gollee, H., and Gawthrop, P. J. Modular neural networks and self-decomposition. *Technical Report CSC-96012*, 1997.

Rosenbaum, C., Klinger, T., and Riemer, M. Routing networks: Adaptive selection of non-linear functions for multi-task learning. *arXiv preprint arXiv:1711.01239*, 2017.

Rosenbaum, C., Cases, I., Riemer, M., and Klinger, T. Routing networks and the challenges of modular and compositional computation. *arXiv preprint arXiv:1904.12774*, 2019.

Roy, A., Saffar, M., Vaswani, A., and Grangier, D. Efficient content-based sparse attention with routing transformers. *arXiv preprint arXiv:2003.05997*, 2020.

Samvelyan, M., Rashid, T., de Witt, C. S., Farquhar, G., Nardelli, N., Rudner, T. G. J., Hung, C.-M., Torr, P. H. S., Foerster, J., and Whiteson, S. The starcraft multi-agent challenge, 2019.

Santoro, A., Raposo, D., Barrett, D. G., Malinowski, M., Pascanu, R., Battaglia, P., and Lillicrap, T. A simple neural network module for relational reasoning. In *Advances in neural information processing systems*, pp. 4967–4976, 2017.

Santoro, A., Faulkner, R., Raposo, D., Rae, J., Chrzanowski, M., Weber, T., Wierstra, D., Vinyals, O., Pascanu, R., and Lillicrap, T. Relational recurrent neural networks. In *Advances in Neural Information Processing Systems*, pp. 7299–7310, 2018.

Shanahan, M. A cognitive architecture that combines internal simulation with a global workspace. *Consciousness and cognition*, 15(2):433–449, 2006.

Shanahan, M. *Embodiment and the inner life: Cognition and Consciousness in the Space of Possible Minds*. Oxford University Press, USA, 2010.

Shanahan, M. The brain's connective core and its role in animal cognition. *Philosophical Transactions of the Royal Society B: Biological Sciences*, 367(1603):2704–2714, 2012.

Shanahan, M. and Baars, B. Applying global workspace theory to the frame problem. *Cognition*, 98(2):157–176, 2005.

Shazeer, N., Mirhoseini, A., Maziarz, K., Davis, A., Le, Q., Hinton, G., and Dean, J. Outrageously large neural networks: The sparsely-gated mixture-of-experts layer. *arXiv preprint arXiv:1701.06538*, 2017.

Van Steenkiste, S., Chang, M., Greff, K., and Schmidhuber, J. Relational neural expectation maximization: Unsupervised discovery of objects and their interactions. *arXiv preprint arXiv:1802.10353*, 2018.

Vaswani, A., Shazeer, N., Parmar, N., Uszkoreit, J., Jones, L., Gomez, A. N., Kaiser, Ł., and Polosukhin, I. Attention is all you need. In *Advances in neural information processing systems*, pp. 5998–6008, 2017.

Vinyals, O., Ewalds, T., Bartunov, S., Georgiev, P., Vezhnevets, A. S., Yeo, M., Makhzani, A., Küttler, H., Agapiou, J., Schrittwieser, J., et al. Starcraft ii: A new challenge for reinforcement learning. *arXiv preprint arXiv:1708.04782*, 2017.

Vinyals, O., Babuschkin, I., Czarnecki, W. M., Mathieu, M., Dudzik, A., Chung, J., Choi, D. H., Powell, R., Ewalds, T., Georgiev, P., et al. Grandmaster level in starcraft ii using multi-agent reinforcement learning. *Nature*, 575 (7782):350–354, 2019.

Wang, S., Li, B., Khabsa, M., Fang, H., and Ma, H. Linformer: Self-attention with linear complexity. *arXiv preprint arXiv:2006.04768*, 2020.

Algorithm 1 Shared Workspace integration with RIMs

Input: Current sequence element, $\boldsymbol{x}_t$ and previous state of the specialist, $\{\boldsymbol{h}_{t-1,k}\},$ for $k \in \{1, \ldots, n_s\}$ and structure of memory as a matrix M with row wise compartmentalized memories, where m_i refers to the state of slot i (total number of slots is n_m).

Step 1: Process image by position p with fully convolutional net
- $\boldsymbol{c}_p = [\mathrm{CNN}(\boldsymbol{x}_t)]_p$
- $\boldsymbol{z}_t = [\boldsymbol{c}_p \; \boldsymbol{e}_p]$ *(concatenate encoding of position to CNN output)*

Step 2: Specialists compete to be selected to update the workspace based on current input
- $\boldsymbol{q}_k = \boldsymbol{h}_{t-1,k}\boldsymbol{W}^q$
- $s_k = \mathrm{softmax}\big(\frac{\boldsymbol{q}_k \boldsymbol{\kappa}}{\sqrt{d_e}}\big)$, where $\boldsymbol{\kappa} = (\boldsymbol{z}_t \boldsymbol{W}^e)^{\mathrm{T}}$
- Construct a set $\mathcal{F}_t$ which contains the indices of the n_{sel} specialists that have the largest s_k
- $\bar{\boldsymbol{h}}_{t,k} = \begin{cases} g_k\left(s_k \boldsymbol{z}_t \boldsymbol{W}^v,\, \boldsymbol{h}_{t-1,k}\right) & k \in \mathcal{F}_t\,, \\ \boldsymbol{h}_{t-1,k} & k \notin \mathcal{F}_t\,, \end{cases}$
- $\boldsymbol{a}_k = s_k \boldsymbol{z}_t \boldsymbol{W}^v \; \forall \; k \in \mathcal{F}_t$ (Scaled Dot Product Attention)

Step 3: Activated specialists write in a shared workspace
- $\widetilde{\boldsymbol{Q}} = \boldsymbol{M}\widetilde{\boldsymbol{W}}^q$
- $\boldsymbol{R} = [\boldsymbol{M}; \boldsymbol{A}]$ where $\boldsymbol{A}$ is the matrix whose rows are the $\boldsymbol{a}_k \forall k \in \mathcal{F}_t$
- $\boldsymbol{M} \leftarrow \mathrm{softmax}\left(\frac{\widetilde{\boldsymbol{Q}}(\boldsymbol{R}\widetilde{\boldsymbol{W}}^e)^{\mathrm{T}}}{\sqrt{d_e}}\right)\boldsymbol{R}\widetilde{\boldsymbol{W}}^v$

Step 4: Broadcast of information from the shared workspace
- $\widehat{\boldsymbol{q}}_k = \bar{\boldsymbol{h}}_{t,k}\widehat{\boldsymbol{W}}^q \quad \forall k \in \{1, \ldots, n_s\}$
- $s_{k,j} = \mathrm{softmax}\left(\frac{\widehat{\boldsymbol{q}}_k \widehat{\boldsymbol{\kappa}}_j}{\sqrt{d_e}}\right)$ where $\widehat{\boldsymbol{\kappa}}_j = (\boldsymbol{m}_j \widehat{\boldsymbol{W}}^e)^{\mathrm{T}} \quad \forall k \in \{1, \ldots, n_s\},\; j \in \{1, \ldots, n_m\}$
- $\boldsymbol{h}_{t,k} = \bar{\boldsymbol{h}}_{t,k} + \sum_j s_{k,j}\widehat{\boldsymbol{v}}_j$ where $\widehat{\boldsymbol{v}}_j = \boldsymbol{m}_j \widehat{\boldsymbol{W}}^v \quad \forall k \in \{1, \ldots, n_s\}$

Appendix

A. Pseudo Codes

Alg. 1 shows the integration of shared workspace with RIMs (Goyal et al., 2019). We replace the direct module to module interaction via attention in RIMs, with shared workspace. Specialists compete to write in the shared workspace, and the contents of the workspace are broadcasted to all the specialists.

Alg. 2 shows the integration of the shared workspace with TIMs (Lamb et al., 2021). Again we replace the direct module to module communication in TIMs, with a shared workspace.

B. Hyperparameters

Table 3 lists the different hyper-parameters.

B.1. Integration with RIMs

RIMs with shared workspace has three set of parameters:

- **Parameters corresponding to Input attention** Parameters for the attention for the k-th specialist $\theta_k = (W_k^q, W^e, W^v)$ corresponding to query, keys, and values respectively. Each specialist has different query parameters but share the same keys and values (which are function of the input). In the table it corresponds to the inp keys, inp values, inp heads respectively.
- **Writing in a shared workspace:** Parameters corresponding to the writing in the memory. Here, we follow the similar mechanisms as in RMC(Santoro et al., 2018), where shared workspace is seen as a Matrix with row wise compartmentalized memories (i.e slots) i.e $\widetilde{\boldsymbol{W}}^q$, $\widetilde{\boldsymbol{W}}^e$, $\widetilde{\boldsymbol{W}}^v$. In the table it corresponds to number of memory slots,

Algorithm 2 Shared Workspace integration with TIMs

Notation: Consider $\boldsymbol{h}_l$ as the output of the l^{th} transformer layer. Let sequence length of original input be T and embedding dimension of transformer be D. Let the transformer be composed of n_b mechanisms and memory be denoted as a matrix M with row wise compartmentalized memories, where m_i refers to the state of slot i (total number of slots is n_m). Consider $\boldsymbol{h}_l^k = \boldsymbol{h}_l[:, (k-1)D/n_b : kD/n_b]$ to be the hidden state of mechanism indexed k at layer l.

Initialization: Convert the raw input $X \in \mathbb{R}^{T \times vocab\_size}$ to $\boldsymbol{h}_0 = positional\_encoding + Embedding(X)$ where $\boldsymbol{h}_0 \in \mathbb{R}^{T \times D}$. Initialize memory matrix M which remains common for all layers in the transformer.

Input to the layer l: $\boldsymbol{h}_{l-1}$ having shape $\mathbb{R}^{T \times D}$

Step 1: Mechanisms compete to be selected to update the workspace based on the input they receive from the previous layer

- $W^c \in \mathbb{R}^{D/n_b \times 1}$
- $c_k = \boldsymbol{h}_{l-1}^k W_k^c \quad \forall k \in \{1, \ldots, n_b\}$
- $c = softmax(concat(c_1, .., c_{n_b}))$, $c \in \mathbb{R}^{T \times n_b}$
- For each time step t in the original sequence of length T, we use the soft score c to select the top n_{sel} mechanisms which would self-attend and write to the memory. Hence generating set $\mathcal{F}_t$ which stores the indices of n_{sel} mechanisms for position $t \in \{1, 2, ..., T\}$. Also construct $c_k^* \in \mathbb{R}^{T \times D/n_b}$ where

$$c_k^*[t, :] = \begin{cases} c[t][k] & k \in \mathcal{F}_t \,, \\ 0 & k \notin \mathcal{F}_t \,, \end{cases}$$

Step 2: Selected mechanisms self-attend and update their hidden state

- $residual_k = \boldsymbol{h}_{l-1}^k$
- $\bar{\boldsymbol{h}}_l^k = c_k^* \odot SelfAttention(\boldsymbol{h}_{l-1}^k) + residual_k \quad \forall k \in \{1, \ldots, n_b\}$

Step 3: Selected mechanisms write on the shared workspace

- Memory matrix M was last modified by mechanisms of layer $l-1$
- Let $\boldsymbol{a}_k = c_k^* \odot \bar{\boldsymbol{h}}_l^k$ and $\boldsymbol{a} = concat(\boldsymbol{a}_1, .., \boldsymbol{a}_{n_b})$. Absorb the first dimension (corresponding to position in the sequence) in the batch dimension by reshaping $\boldsymbol{a}$. Perform the same steps as in algorithm 1.
- $\widetilde{\boldsymbol{Q}} = \boldsymbol{M}\widetilde{\boldsymbol{W}}^q$
- $\boldsymbol{R} = [\boldsymbol{M}; \boldsymbol{A}]$ where $\boldsymbol{A} = \boldsymbol{a}\boldsymbol{W}^v$
- $\boldsymbol{M} \leftarrow \text{softmax}\left(\frac{\widetilde{\boldsymbol{Q}}(\boldsymbol{R}\widetilde{\boldsymbol{W}}^e)^{\mathrm{T}}}{\sqrt{d_e}}\right)\boldsymbol{R}\widetilde{\boldsymbol{W}}^v$

Step 4: Broadcast of information from the shared workspace

- Reshape the new memory to bring back the sequence dimension. Perform the same steps as in algorithm 1.
- $\widehat{\boldsymbol{q}}_k = \bar{\boldsymbol{h}}_l^k \widehat{\boldsymbol{W}}^q \quad \forall k \in \{1, \ldots, n_b\}$
- $s_{k,j} = \text{softmax}\left(\frac{\widehat{\boldsymbol{q}}_k \widehat{\boldsymbol{\kappa}}_j}{\sqrt{d_e}}\right)$ where $\widehat{\boldsymbol{\kappa}}_j = (\boldsymbol{m}_j \widehat{\boldsymbol{W}}^e)^{\mathrm{T}} \quad \forall k \in \{1, \ldots, n_b\},\ j \in \{1, \ldots, n_m\}$
- $\boldsymbol{h}_l^k = \bar{\boldsymbol{h}}_l^k + \sum_j s_{k,j} \widehat{\boldsymbol{v}}_j$ where $\widehat{\boldsymbol{v}}_j = \boldsymbol{m}_j \widehat{\boldsymbol{W}}^v \quad \forall k \in \{1, \ldots, n_b\}$

number of memory heads, size of attention head, key size and number of mlp layers in attention. These are the same hyper-paramter as in RMC (Santoro et al., 2018). We tried two different set of hyper-parameters (a) where we only have a single slot and (b) where we have 4 slots.

- **Broadcast of Information from the shared workspace**: In this process, the information in the workspace gets broadcasted to all the specialists such that each specialist produces a query, and the keys and values are a function of the memory state. Each specialist gets information from the memory according to its query, and this information is used to update the state of each specialist in a residual fashion. This corresponds to the parameters of $\widehat{\boldsymbol{W}}^v$, $\widehat{\boldsymbol{W}}^q$, $\widehat{\boldsymbol{W}}^e$ in the table i.e memory attention heads, memory attention keys, and memory attention values. We did not do any hyper-parameter search for these hyper-parameters.

Resources Used:

- For vision tasks like Sort-of-clever, Equilateral triangle, CIFAR classification, it takes about 6 hours to run 200 epochs on V100 (32G) GPU.
- It takes about 2 days to train the proposed model on bouncing ball task for 100 epochs on V100 (32G) GPU. We did not do any hyper-parameter search specific to a particular dataset (i.e 4Balls or 678Balls or Curtain Task). We ran the proposed model for different number of memory slots (i.e 2/4/8) for all the different datasets.

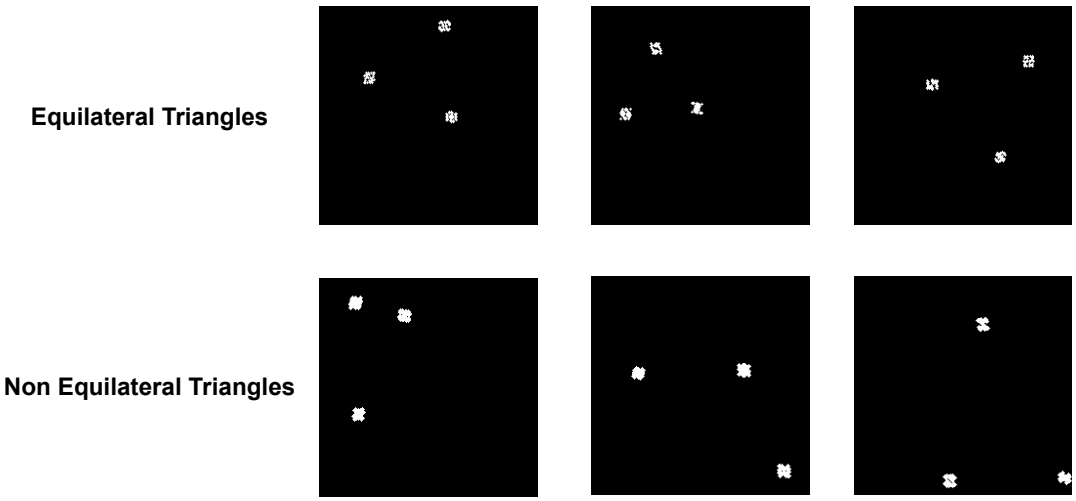

Figure 6. A demonstration of the detecting equilateral triangles task.

- For Starcraft task, it takes about 5 days to train on V100 (16G) GPU with batch size of 4.

C. Implementation Details

Writing Information in the shared workspace. While writing information to the shared workspace, we update the workspace using a gating mechanism as proposed in (Santoro et al., 2018). The gating mechanism consists of *input* and *forget* gates. Let $\boldsymbol{M}^{t-1}$ and $\boldsymbol{M}^{t}$ be the previous and updated memory matrix respectively. Let $\boldsymbol{M}$ be the result of the attention mechanism as described in step 2 of section 2.1. Let $\boldsymbol{X}_{1\ldots n_s}$ be the input to n_s specialists. The gating mechanism can be formulated as follows.

$$
\begin{aligned}
\bar{\boldsymbol{X}} &= \frac{1}{n_s}\sum_{i=1}^{n_s}\text{relu}(\boldsymbol{X}_i \times \boldsymbol{W}^1) \\
\boldsymbol{K} &= \bar{\boldsymbol{X}} + \tanh(\boldsymbol{M}^{t-1}) \\
\boldsymbol{I} &= \text{sigmoid}(\boldsymbol{K}\boldsymbol{W}^I) \\
\boldsymbol{F} &= \text{sigmoid}(\boldsymbol{K}\boldsymbol{W}^F) \\
\boldsymbol{M}^t &= \boldsymbol{I} \times \tanh(\boldsymbol{M}) + \boldsymbol{F} \times \boldsymbol{M}^{t-1}
\end{aligned}
$$

Here, $\boldsymbol{I}$ and $\boldsymbol{F}$ indicate the input and forget gates respectively. Note that $\boldsymbol{W}^1$ is shared across all n_s specialists.

D. Transformer Tasks

D.1. Detecting Equilateral Triangles

A demonstration of this task can be found in figure 6. We use images of size 64×64 for this task. Our training dataset consists of 50000 examples and we evaluate on 10000 examples. We follow the same setup as vision transformers (Dosovitskiy et al., 2020) for this task. We divide the image into patches of size 4×4, this sequence of patches is fed as input to a 4-layered transformer along with the CLS token which is used for classification. We set hidden dim to 256 and ffn dim to 512. For the proposed model (TR+SSW, TR+HSW), We use a query and key size of 32, and value size of 64. We use 4 heads during reading from and writing into the shared workspace which consist of 8 memory slots. For the baseline models (TR, TR + HC, STR), we use query, key and value size of 64 and 4 heads. For training, we use a batch size of 64. We train the model for 200 epochs using Adam optimizer with a learning rate of 0.0001. We anneal the learning rate using cosine annealing.

Table 3. Generic Hyperparameters for the proposed model (for RIMs)

Parameter	Value
Number of specialists (n_s)	6
Size of each specialist	85
Number of memory slots (n_m)	
Optimizer	Adam(Kingma & Ba, 2014a)
learning rate	$1 \cdot 10^{-4}$
batch size	64
Inp keys	64
Inp Values	85
Inp Heads	4
Inp Dropout	0.1
Number of memory slots	4
Number of memory heads	1
Size of attention head	32
Key size	32
Number of MLP layers in Attention	3
Gate Style	'unit'
Memory Attention Heads	4
Memory Attention keys	32
Memory Attention Values	32

D.2. Sort-of-clevr

Figure 7 shows a sample from this dataset. The images in this dataset are of size 75×75. Each question is encoded into 11 bits. The first 6 bits indicate color, the next 2 bits indicate question type (relational or non-relational), and the remaining 3 bits indicate question subtype (according to figure 7). We use a 4-layered transformer for this task with hidden dim set to 256 and ffn dim set to 512. For the proposed model (TR+SSW, TR+HSW), We use a query and key size of 32, and value size of 64. We use 4 heads during reading from and writing into the shared workspace which consists of 8 memory slots. For the baseline models (TR, TR + HC, STR), we use query, key and value size of 64 and 4 heads. We encode the 11 bit question into a 256 dimensional vector representation and concatenate it with the sequence of 15×15 sized patched obtained from the image. We use the representation corresponding to the CLS token for classification. We train the model using cross-entropy loss. We use a batch size of 64 and train the model for 100 epochs. We use Adam optimizer with a learning rate of 0.0001 for training.

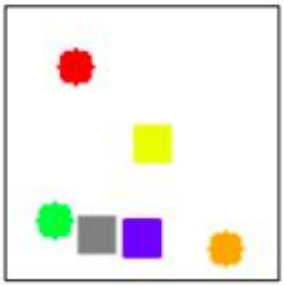

Relational questions:

1. What is the shape of the object closest to the red object? ⇒ square
2. What is the shape of the object furthest to the orange object? ⇒ circle
3. How many objects have same shape with the blue object? ⇒ 3

Non-relational questions:

1. What is the shape of the red object? ⇒ Circle
2. Is green object placed on the left side of the image? ⇒ yes
3. Is orange object placed on the upside of the image? ⇒ no

Figure 7. A sample from the sort-of-clevr dataset.

D.3. CATER: Object Tracking

Each CATER video consists of about 300 frames of size 224×224. We first sample frames at a sampling rate of 6 which results in 50 frames. From these 50 frames, we stack 5 consecutive frames together and pass each stack through a 18 layered resnet. The corresponding sequence of 10 frames is passed as input to the transformer. We use a 6-layered transformer with hidden dim set to 512 and ffn dim set to 2048. For the proposed model (TR+SSW, TR+HSW), We use a query and key size of 32, and value size of 64. We use 8 heads during reading from and writing into the shared workspace which consists of 8 memory slots. For the baseline models (TR, TR + HC, STR), we use query, key and value size of 64 and 8 heads.

D.4. MultiMNIST Generation

Table 4. Hyperparameters for MultiMNIST Task

Parameter	Value
Common Parameters	
Optimizer	Adam(Kingma & Ba, 2014a)
Learning rate	$1 \cdot 10^{-3}$
Batch size	12
Number of attention heads	8
TR	
Size of transformer layer	256
TIMs	
Number of mechanisms	4
Size of mechanism	48
TIMs+SW	
Number of mechanisms	4
Size of mechanism	40
Number of memory slots	2
Size of memory slots	160
Memory Attention Heads	8
Gate Style	'unit'
Number of MLP layers in Attention	2

In this task, we train an Image Transformer (Parmar et al., 2018) (pixel-by-pixel, raster-order generative model) for next pixel prediction task on the "MultiMNIST dataset"

Each 32×32 image in this dataset is made up of four randomly selected (and augmented) MNIST digits (resized to 32×8) placed side-by-side as shown in figure 8. The digits themselves are selected independently of one-another.

The main aim of creating such a task is to observe the working of independent mechanisms in architectures such as TIMs (Lamb et al., 2021). Each image in the MultiMNIST dataset can be broken down into different sets of independent spatial components. Since the digits which make up the image are independently selected, the joint distribution of pixel intensities in any one of the four sections of the image is statistically independent of the pixel intensities in any other section of the image. Moreover each section of the image can be further broken down into independent spatial components: one that pertains to the background and one that pertains to the foreground.

It is expected that a monolithic architecture (having a single computational unit) would have to devote a significant portion of its training to learn the statistical independence between the different constituents of the image. On the other hand, architectures made up of sparsely interacting independent mechanisms have a natural way of capturing such statistical independence. A division of labour where each mechanism is focused on the generation of a distinct independent constituent of the image should allow for better generalization on the test set. Once the generation of a constituent is completed, the task can be handed over to some other mechanism based on current position in the image.

Table 5. **MultiMNIST Generation Task:** We report cross-entropy loss between the generated pixel values and the true pixel values on the test set of MultiMNIST Generation Task (smaller numbers are better)

Model	Loss
TR	0.000058
TIMs (4 mechanisms)	0.000050
TIMs+SW (4 mechanisms)	0.000042

For this experiment we train a standard transformer with shared parameters across all layers (denoted by TR), TIMs (Lamb et al., 2021) with 4 mechanisms, and a modified version of TIMs with 4 mechanisms where the pair-wise communication between the mechanisms is replaced by communication via a shared workspace (denoted by TIMs+SW).

Training. We follow the minGPT Image Transformer setup (Karpathy, 2020) for our experiments. All three of the configurations have 8 layers, 8 heads for multi-headed attention and use the exact same parameter initialization and base architecture. We train all three of the models for 20 epochs.

In the TR model, all of the 8 monolithic layers share the same set of parameters. In TIMs and TIMs+SW, the first two layers are the standard monolithic layers having shared parameters. The middle four layers in both of these architectures are modular layers with four mechanisms. These four layers share the same set of parameters. In the case of TIMs+SW, the four mechanisms in these layers communicate via a shared workspace (having 2 memory slots). This shared workspace is common for all four middles layers and is absent in TIMs where the mechanisms communicate via pair-wise competition as proposed in the original paper. TIMs and TIMs+SW architectures are concluded by two more monolithic layers which again share the same parameters.

For all three models to have comparable number of parameters, we chose the transformer embedding dimension to be 256 for TR model, 192 for TIMs model and 160 for TIMs+SW model. In TIMs and TIMs+SW, the embedding dimension is divided equally among the four specialists. Each memory slot in the shared workspace of the TIMs+SW model has a 160 dimensional embedding and the model uses four heads to perform read and write operations on the shared workspace. Total number of parameters for all three architectures lie between 1M and 1.8M.

Results. We observe the best cross-entropy loss in 20 epochs on the test set of the MultiMNIST dataset for the next pixel prediction task in the table 5. We further plot the sixth layer "mechanism activation score" of TIMs and TIMs+SW while generating the first four images of the test set in the best epoch (shown in figure 9). We call these plots as Mechanism Activation Maps.

From left to right, each Mechanism Activation Map is divided into four sections of size 32×32 and each section belongs to a unique mechanism. A mechanism which is activated during the generation of a particular pixel in a test image will have a non-zero activation value at the same location in its section of the activation map. These activation scores are produced as a result of a soft competition between different mechanisms and the mechanism with higher score will have more control over the state update of the transformer. The degree of activation is highlighted by the pixel intensities in these plots.

It is clear from these plots that the TIMs model is unable to devise an ideal division of labour between its mechanisms. Most of the computation is handled by the second mechanism in all four images. Upon closer look, one can notice that there are four dark stripes present in the activation map of the second mechanism and four white stripes present in the activation map of the fourth mechanism at the same location which suggests that the model has somewhat understood the boundaries of the four sections of the image. Yet most of the computation is still handled by the second mechanism, even at the boundaries of the four sections in the image, indicating that the model is unable to properly utilize three of its four mechanisms.

Using a shared workspace on the other hand shows a drastic improvement in the division of labour among different mechanisms. The second mechanism gets activated only near the center of each of the four sections of the image. This is intuitive since most of the digits in the images of this dataset lie near to the center of their section. Therefore it seems that the second mechanism is concerned with the generation of the digits themselves.

Most interesting are the plots of mechanisms 3 and 4. It seems that the model has divided the non-digit area in the image into two parts, one which marks the boundary between adjacent sections and one which marks the top and bottom of the image. This indicates that 1) the model clearly understands the boundaries between different sections of the image 2) the model understands that the top and bottom portions of each section function similarly since it is highly unlikely to find a digit there irrespective of which section it is.

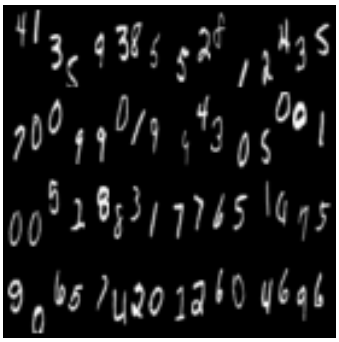

Figure 8. A randomly selected batch of 16 images from the MultiMNIST generation dataset (4 rows and 4 columns)

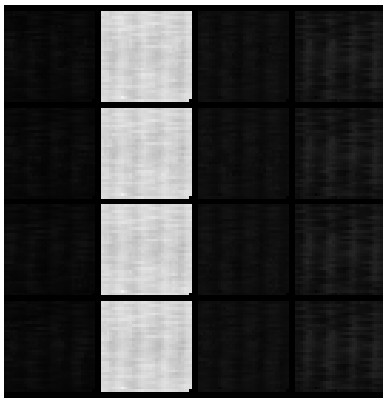

(a) Mechanism Activation Maps for TIMs

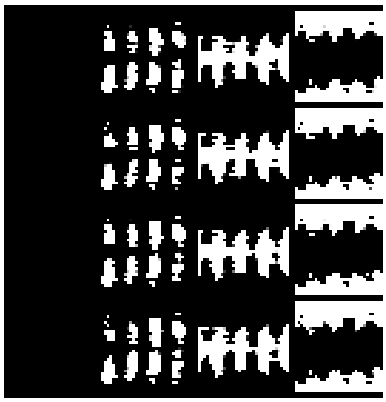

(b) Mechanism Activation Maps for TIMs+SW

Figure 9. Mechanism Activation Maps for TIMs and TIMs+SW

Further, the activation maps in TIMs+SW are almost black and white, which means that at a given position, the computation is single handedly completed by a single mechanism. This indicates that by using a shared workspace, different mechanisms become specialists of different parts of the image. Such a case was not possible in TIMs suggesting that global-level communication is crucial for allowing the mechanisms to specialize. The losses also show that that global-level communication allows for a mixture-of-experts to generalize better.

E. Using Workspace for language Modelling

We train our models on the WikiText-103 dataset by posing a language modeling problem. The dataset is divided into train, test and validation sets which are composed out of 28,475, 60 and 60 articles respectively. The total number of tokens in the train set is more than 103 million, hence the name of the dataset. This dataset retains numbers, punctuation and case.

Training. We train our models for 15 epochs for the next word prediction task on the WikiText-103 dataset and report the perplexity on the validation set. We show the results using TIMs (Lamb et al., 2021) with 4 mechanisms and TIMs+SW with 4 mechanisms (where we replace the pairwise communication in TIMs with communication via a shared workspace like in the MultiMNIST experiment). We modify the FAIRSEQ (Ott et al., 2019) transformer language model class for all of our experiments.

For TIMs+SW, we train and test two different variants: TIMs+SSW uses soft attention to generate the activation scores of competing independent mechanisms whereas TIMs+HSW uses top-k attention with k=2.

Since in this test, our aim is to compare the performance of the two models for the language modeling task, the architectures are only made up of a transformer decoder. In both of the models, there are 8 transformer decoder layers divided into 3 sets. The first 2 layers are standard monolithic decoder layers which share the same parameters. The next 4 layers are modular

layers (TIMs layers or TIMs+SW layers depending on the model choice). These layers also share the same parameters among themselves. The last 2 layers are again standard monolothic decoder layers, both sharing the same parameters.

The inputs to the network are 1024 dimensional word embeddings, input to a transformer layer of dimension 1024 and feed forward dimension of 2048.

Both of the networks have 8 attention heads with head dimension of 128. The total transformer layer size of $8 \times 128 = 1024$ is equally divided among the four mechanisms. In the case of TIMs, these mechanisms (in layers 3,4,5) interact via pair-wise communication, whereas in TIMs+SSW and TIMs+HSW, these mechanisms interact via a shared workspace. The shared workspace has 2 memory slots, each 1024 dimensional, having 4 attention heads for reading and writing.

Table 6. Hyperparameters for WikiText-103 Language Modeling Task

Parameter	Value
Common Parameters	
Optimizer	Adam(Kingma & Ba, 2014a)
Learning rate	$5 \cdot 10^{-4}$
Adam betas	$0.99, 0.98$
Weight decay	0.01
lr scheduler	'inverse square root'
Max tokens per gpu	3078
Batch size multiple	8
Number of attention heads	8
Transformer layer size	1024
Number of Mechanisms	4
Update frequency	4
Number of warmup updates	4000
Starting Warmup lr	$1 \cdot 10^{-7}$
TIMs+SSW	
Number of memory slots	2
Size of memory slots	1024
Memory Attention Heads	4
Gate Style	'unit'
Number of MLP layers in Attention	3
top-k competition	False
TIMs+HSW	
Number of memory slots	2
Size of memory slots	1024
Memory Attention Heads	4
Gate Style	'unit'
Number of MLP layers in Attention	3
top-k competition	True, k=2

Results. We plot the perplexity (per epoch) on the validation set. All models have comparable number of parameters (within a 10% difference). We note that TIMs performs poorly on this dataset but adding shared workspace improves the performance consistently. We also note that sparsity indeed helps as TIMs+HSW performed the best.

F. Bouncing Ball

The dataset consists of 50,000 training examples and 10,000 test examples showing $\sim$50 frames of either 4 solid balls bouncing in a confined square geometry (*4Balls*), 6-8 balls bouncing in a confined geometry (*678Balls*), 3 balls bouncing in a confined geometry with an occluded region (*Curtain*), or balls of different colors (*Colored 4Balls*) and (*Colored 678Balls*).

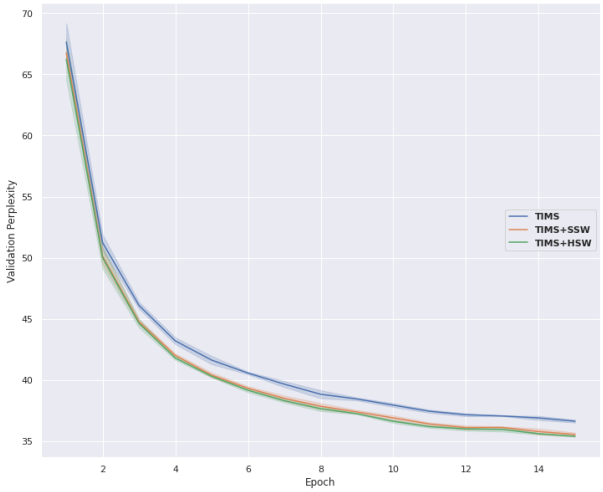

Figure 10. Per epoch validation perplexity for TIMs, TIMs+SSW, TIMs+HSW for wikitext-103 language modeling task

We trained baselines as well as proposed model for about 100 epochs. We use the same architecture for encoder as well as decoder as in (Van Steenkiste et al., 2018). Hyper-parameters specific to the proposed architecture are listed in Tab. 3.

G. MultiAgent Starcraft

The Starcraft2 Environment we use is a modified version of the SMAC-Env proposed in Samvelyan et al. (2019) and built on PySC2 wrapper around Blizzard SC2 API (Vinyals et al., 2017). Starcraft2 is a real-time-strategy (RTS) game where players are tasked with manufacturing and controlling armies of *units* (airborne or land-based) to defeat the opponent's army (where the opponent can be an AI or another human). The players must choose their *alien race*[3] before starting the game; available options are *Protoss*, *Terran* and *Zerg*. All unit types (of all races) have their strengths and weaknesses against other unit types, be it in terms of maximum health, shields (Protoss), energy (Terran), DPS (damage per second, related to weapon cooldown), splash damage, or manufacturing costs (measured in *minerals* and *vespene gas*, which must be mined).

The key engineering contribution of Samvelyan et al. (2019) is to repurpose the RTS game as a multi-agent environment, where the individual units in the army become individual agents[4]. The result is a rich and challenging environment where heterogeneous teams of agents must defeat each other in melee and ranged combat. The composition of teams vary between *scenarios*, of which Samvelyan et al. (2019) provide a selection. Further, new scenarios can be easily created with the SC2MapEditor, which allows for practically endlessly many possibilities.

We build on Samvelyan et al. (2019) by modifying their environment to better expose the transfer and out-of-distribution aspects of the domain by (a) standardizing the state and action space across a large class of scenarios and (b) standardizing the unit stats to better reflect the game-defined notion of hit-points. We do not fix the number of agents in the environment and allow for agents to dynamically enter or exit the environment.

Training. We adapt the encoder and decoder architecture to match the state representation by including circular convolutions. Predicting the next state entails predicting images of binary friendly markers, categorical unit type markers and real valued HECS markers. Accordingly, the loss function is a sum of a binary cross-entropy term (on friendly markers), a categorical cross-entropy term (on unit-type markers) and a mean squared error term (on HECS markers). [5]

[3]Please note that this is a game-specific notion.

[4]Note that this is rather unconventional, since each player usually controls entire armies and must switch between macro- and micro-management of units or unit-groups.

[5]Note the training setup is same as in (Rahaman et al., 2020), and have been copied from the appendix of (Rahaman et al., 2020) (with permission).

G.1. Standardized State Space for All Scenarios

In the environment provided by Samvelyan et al. (2019), the dimensionality of the vector state space varies with the number of friendly and enemy agents, which in turn varies with the scenario. While this is not an issue in the typical use case of training MARL agents in a fixed scenario, it is not convenient for designing models that seamlessly handle multiple scenarios. In the following, we propose an alternate state representation that preserves the spatial structure and is consistent across multiple scenarios.

Instead of representing the state of an agent a with a vector of variable dimension, we represent it with a multi-channel *polar image* I^a of shape $C \times I \times J$, where C is the number of channels and (I, J) is the image size. Given the *radial* and *angular* resolutions ρ and φ (respectively), the pixel coordinate $i = 0, ..., I-1, j = 0, ..., J-1$ corresponds to coordinates $(i \cdot \rho, j \cdot \varphi)$ with respect to a polar coordinate system centered on the agent a, where the positive x-axis ($j = 0$) points towards the east. Further, the field of view (FOV) of an agent is characterized by a circle of radius $I \cdot \rho$ centered on the agent at 2D game-coordinates $\boldsymbol{x}^a = (x_1^a, x_2^a)$, to which the Starcraft2 API (Vinyals et al., 2017) provides raw access.

The polar image I^a therefore provides an agent-centric view of the environment, where pixel coordinates i, j in I^a can be mapped to global game coordinates $\boldsymbol{x} = (x_1, x_2)$ in FOV via:

$$x_1 = i \cdot \rho \cos[j \cdot \varphi] + x_1^a \tag{1}$$

$$x_2 = i \cdot \rho \sin[j \cdot \varphi] + x_2^a \tag{2}$$

In what follows, we denote this transformation with T_a, as in $T_a(i, j) = (x_1, x_2)$.

Now, the channels in the polar image can encode various aspects of the observation; in our case: friendly markers (one channel), unit-type markers (nine channels, one-hot), health-energy-cooldown-shields (HECS, four channels) and terrain height (one channel). As an example, let us consider the friendly markers, which is a binary indicator marking units that are friendly. If we have an agent at game position (x_1, x_2) that is friendly to agent a, then we would expect the pixel coordinate $(i, j) = T_a^{-1}(x_1, x_2)$ of the corresponding channel in the polar image I^a to be 1, but 0 otherwise. Likewise, the value of I at the channels corresponding to HECS at pixel position i, j gives the HECS of the corresponding unit[6] at $T_a(i, j)$. This representation has the following advantages: **(a)** it does not depend on the number of units in the field of view, **(b)** it exposes the spatial structure in the arrangement of units which can naturally processed by convolutional neural networks (e.g. with circular convolutions).

Nevertheless, it has the disadvantage that the positions are *quantized* to pixels, but the euclidean distance between the locations represented by pixels (i, j) and $(i, j + 1)$ increases with increasing i. Consequently, this representation may not remain suitable for larger FOVs.

Further, this representation is also appropriate for the action space. Given an agent, we represent the one-hot categorical actions of all friendly agents in FOV as a multi-channel polar image. In this representation, the pixel position i, j gives the action taken by an agent at at position $T_a(i, j)$. Unfriendly agents get assigned an "unknown action", whereas positions not occupied by a living agent are assigned a "no-op" action.

G.2. Standardized Unit Stats

At any given point in time, an active unit in Starcraft2 has certain *stats*, e.g. its health, energy (Terran), shields (Protoss) and weapon-cooldown (for armed units). A large and expensive unit-type like the Colossus has more max-health (*hit-points*) than smaller units like Stalkers and Marines[7]. Likewise, unit-types differ in the rate at which they deal damage (measured in damage-per-second or DPS, excluding splash damage), which in turn depends on the cooldown duration of the active weapon.

Now, the environment provided by Samvelyan et al. (2019) normalizes the stats by their respective maximum value, resulting in values between 0 and 1. However, given that different units may have different normalization, the stats are rendered incomparable between unit types (without additionally accounting the unit-type). We address this by standardizing stats (instead of normalizing) by dividing them by a fixed value. In this scheme, the stats are scaled uniformly across all unit-types, enabling models to directly rely on them instead of having to account for the respective unit-types.

[6] If health drops to zero, the unit is considered dead and the representation does not differentiate between dead and absent units.

[7] These stats may change with game-versions, and are catalogued here: https://liquipedia.net/starcraft2/Units_(StarCraft).

Model Hyperparameter	Value
Proposed Method (Shared Workspace)	
Inp keys	64
Inp Values	128
Inp Heads	4
Inp Dropout	0.1
Number of memory slots	1
Number of memory heads	4
Size of attention head	64
Key size	32
Number of MLP layers in Attention	3
Gate Style	'unit'
Memory Attention Heads	4
Memory Attention keys	32
Memory Attention Values	32
RMC (Santoro et al., 2018)	
Number of attention heads	4
Size of attention head	128
Number of memory slots	1
Key size	16
LSTM (Hochreiter & Schmidhuber, 1997)	
Hidden size	2048

Table 7. Hyperparameters used for various models on the Starcraft2 task. Hyperparameters not listed here were left at their respective default values.

G.3. Encoder and Decoder for Starcraft2

G.3.1. TRAINING

All models were trained using Adam (Kingma & Ba, 2014b) with an initial learning rate 0.0003. We use Pytorch's (Paszke et al., 2019) `ReduceLROnPlateau` learning rate scheduler to decay the learning rate by a factor of 2 if the validation loss does not improve by at least 0.01% over the span of 5 epochs. We train all models for 200 epochs and finally select the checkpoint with the lowest validation loss (i.e. we early stop). We train all models with batch-size 4 (Starcraft2).

G.3.2. STARCRAFT2 MODELS

The hyperparameters we used can be found in Table 7. Note that we only report models that attained a validation loss similar to proposed method (Small LSTMs and RIMs fail to achieve that).

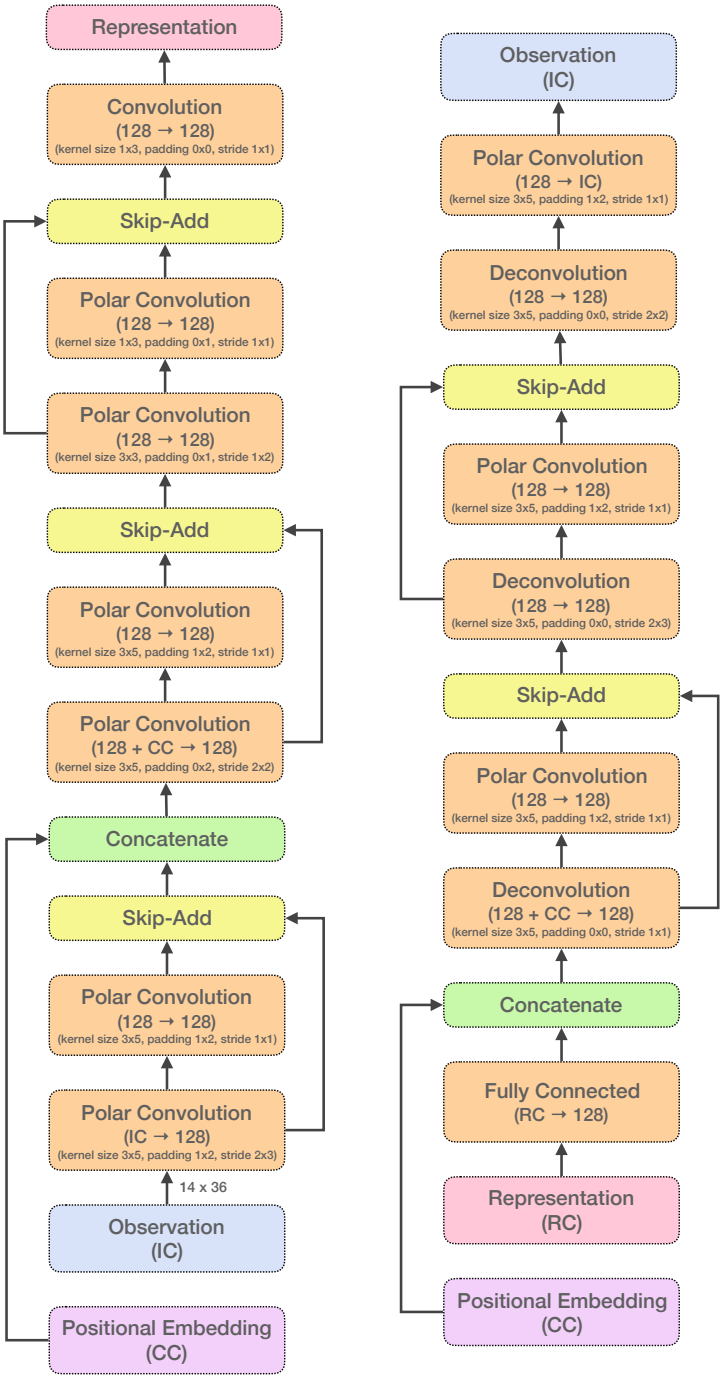

(a) **Encoder** (b) **Decoder**

Figure 11. Encoder and Decoder architectures for the Starcraft2 task.